Edge-Guided Image Gap Interpolation Using Multi-scale Transformation

Bahareh Langari, Saeed Vaseghi, Ales Prochazka, Babak Vaziri, Farzad Tahmasebi Aria

Abstract — **This paper presents improvements in image gap restoration through incorporation of edge-based directional interpolation within multi-scale pyramid transforms. Two types of image edges are reconstructed; (a) the local edges or textures, inferred from the gradients of the neighbouring pixels and (b) the global edges between image objects or segments, inferred using Canny detector. Through a process of pyramid transformation and down-sampling, the image is progressively transformed into a series of reduced size layers until at the pyramid apex the gap size is one sample. At each layer an edge 'skeleton' image is extracted for edge-guided interpolation. The process is then reversed; from the apex, at each layer, the missing samples are estimated (an iterative method is used in the last stage of up-sampling), up-sampled and combined with the available samples of the next layer. Discrete cosine transform and a family of discrete wavelet transforms are utilized as alternatives for pyramid construction. Evaluations over a range of images, in regular and random loss pattern, at loss rates of up to 40%, demonstrate that the proposed method improves PSNR by 1 to 5 dB compared to a range of best published works.**

Index Terms—Error concealment, multi-scale DCT/DWT pyramid, edge detection, image gap recovery, packet loss concealment.

I. Introduction

Image gap restoration have a wide range of applications that includes in-painting of missing or damaged segments in still images or the replacement of image data packet lost in transmission. Further examples of applications and environments where image gap restoration can be usefully applied are enhancement of distorted biomedical signals [1], restoration of archived damaged images [2] and packet loss concealment over internet protocol (IP) networks [3].

A main current application of image gap restoration is packet loss concealment. Packet loss errors may occur due to network congestions or due to signal loss in mobile devices. IP networks are best-effort environments [4,5] where the packet delivery is not guaranteed. The rapid growth in demand for relatively high bandwidth image/video streaming applications over IP networks motivates the need for packet loss recovery and concealment in order to provide more reliable network services and more acceptable user experience [6].

There are three broad approaches for mitigating the loss of quality in received images due to packet loss: (a) automatic request for retransmission (ARQ) of the lost packets, (b) error control via forward error correction (FEC) methods and (c) error concealment (EC) methods. The first method retransmits a copy of the damaged/lost packet and results in an increase in bandwidth and delay proportional to error rate [5]. This method can be used on request for retransmission in networks where there is an interaction between sender and receiver. The second category of methods, FEC, employs error correction coding to recover lost pixels from the received information. This implies that the pixel values in successive blocks of images would be coded, combined and/or spread over several successive packets. This method also involves an increase in bandwidth and delay [4-6]. The third category of methods, EC, is receiver-based signal processing methods that aim to replace the lost packets with estimates obtained from the received packets. To recover lost packets from the neighbouring pixel values, EC methods utilise the observation that images often contain high spatial structures, correlations and recurring textures and patterns [7-16].

Among the three solutions listed above for packet loss recovery, an effective EC would be most beneficial as it does not require an increase in bandwidth, in contrast retransmission and FEC requires additional bandwidth and perhaps delay. Furthermore, retransmission and FEC techniques are not immune to errors. In addition, EC methods can be coded as stand-alone apps and deployed in networks or used as embedded applications on the receiver handsets/terminals; they do not require an international telecommunication union (ITU) approved standard. Therefore, spatial EC image gap restoration is the category of solution explored in this paper.

At their core, image EC computation algorithms often involve two distinct processes: (a) image transformation and (b) extrapolation or interpolation of missing gaps.

For selection of the domain in which image is interpolated, the common choices vary from direct interpolations over raw spatial domain pixels [8,18], to methods which operate on transformation of images using discrete cosine transform (DCT) [7] or discrete wavelet transforms (DWT) [17]. EC methods using combination of spatial and frequency domains

are investigated in [20, 21, 26]. In this paper image restoration is investigated within a pyramid structure that lends itself to the use of the DCT or various families of DWT as the kernel function.

The main justification for the choice of pyramid as the framework for interpolation is one of pragmatic; a relatively large gap at the base is reduced to a single sample at the apex which can be conveniently interpolated. The result can then be progressed downwards towards the pyramid base through a set of repeated and scaled-up operations [7,19]. In [22] a hybrid image reconstruction (HIR) algorithm is developed that the modeling strength of the parametric and nonparametric techniques are combined within a multiscale framework.

For EC interpolation methods, the choice is between non-directional methods such as bilinear interpolation [7,10,12,16 ,23,27] and directional interpolation [8,11,13-15]. However, each method has some drawback. Bilinear and non-directional techniques are able to recover the smooth area but fail to restore the visually important edge information. An example of non-directional is basic spatial interpolation methods which use a weighted average of the neighbouring pixels to recover the lost gap. Although in this way satisfactory result is achieved in the smooth areas, the performance around the edges can be blurred [12]. More recently, Zhai *et al*. [7] proposed a method which is a combination of a Bayesian framework and a DCT transform on a multi-scale EC platform. A further Bayesian estimation method based on an adaptive linear prediction put forward by Liu *et al*. [23]. Missing pixels are reconstructed sequentially, pixel by pixel, utilising linear prediction, with the order of the predictor being determined by adopting a Bayesian information criterion (BIC).

On the other hand while directional interpolation methods do well in recovery of the edges, they suffer from leaving stripe-shaped artifacts in the smooth part of the image. Such as, Edge-oriented directional interpolations, that have been investigated in [13-15]. Asheri et al. [8] proposed an algorithm called novel adaptive Gaussian process (NAGP). The missing areas are divided into different sections based on multiple hypothesized edges. Then, each section is restored separately with adaptive kernel functions. Although some edge distortion are avoided, but the difficult process of division of missing block may introduce false borders. Multiple edges are also addressed in [38], where several directional interpolations are combined according to the visual clearness (VC) of the edges. Even though complicate edges can be reconstructed, it is hard to accurately determine the location and the VC of the edges. In [24] an adaptive method is proposed to develop an EC algorithm that benefits from a combination of directional and non-directional methods. Two steps are involved in this technique; at the first stage the type of the error block (EB) is detected and classified into one of the three; uniform, texture or edge groups. Then, a suitable EC method is applied to each category.

A further approach to SEC is block-matching based, described in [16] searches for the best similar macro-block (MB) in the image to replace the missing MB, using a technique called best neighbourhood matching, but the computational complexity of this technique is quite high. In [25] vector-valued image regularization based on variations methods and partial differential equation are introduced for image enhancement and in-painting. Another major group of error concealment technique is based on sparse linear predictions [26]. In [27] a linear predictor is used to restore the missing MB areas sequentially. An adaptive procedure, which is a combination of sparsity and a missing data imputation approach, utilized to compute the coefficients. From the analysis above, it is been observed even though a lot of attempts have been made to preserve edges in the corrupted blocks along with texture, these proposed algorithms often fail when more than one edge is involved or a successive sequence of blocks are corrupted. Therefore it is evident to obtain high quality image restoration results, it is of paramount importance to include the image edge information.

The preliminary idea of the proposed method suggested in [42], a complete version and more results is proposed in this paper. The main contribution of this work are: (1) improvements in multi-scale image gap restoration obtained through incorporation of the local texture interpolation and global edge-guided interpolation based on Canny edge detector, (2) introduction of edge 'skeleton' layers within pyramid transform structures, (3) Comparison of DCT and families of DWT as the basis for pyramid transformation and (4) use of iterative methods for improving various layers of pyramid reconstruction.

The remainder of this paper is organized as follows. In section II, the theory and implementation of the proposed multi-scale edge-guided image restoration method is introduced. The experimental evaluation results and comparison with published works are presented in section III. Finally section IV presents concluding remarks.

II. THE PROPOSED IMAGE GAP CONCEALMENT

A. Multi-Scale Pyramid Discrete Cosine and Wavelet Transforms

The multi-scale pyramid processing method, illustrated in Fig. 1 (DCT) and Fig. 2 (DWT) progressively decomposes image macro-blocks (MB) into four spectral quadrants; LL, LH, HL, HH where L and H denote low and high frequency halves of the spectrum respectively. After the first stage of decomposition, at each subsequent down-sampling and decomposition stage, the LL quadrant is further decomposed into four spectral quadrants until the macro-block is reduced to a single pixel as shown in Fig. 1. For a MB of size 8×8, three stages of decomposition and down-sampling reduces the MB to one pixel. The pyramid transformation can be expressed as:

$$f_{p,q}^{i} = \sum_{m=0}^{M_i-1} \sum_{n=0}^{N_i-1} f_{m,n}^{i-1} \, \emptyset(m,n,p,q) \;\; i = 1, \dots, N \qquad (1)$$

where $f_{p,q}^{i}$ is the transformation layer i and the function $\emptyset$ is the transformation kernel - at the pyramid base level for layer $0, i = 0,\ f_{m,n}^{0} = image(m,n).$

For example the DCT pyramid layers are obtained as:

$$f_{p,q}^{i} = IDCT2\left(DCT2\left(f_{m,n}^{i-1}\right)\right) \quad (2)$$

where for an $M_i \times N_i$ matrix, at the i^{th} layer is defined as:

$$f_{p,q}^{i} = a_p a_q \sum_{m=0}^{M_{i-1}-1} \sum_{n=0}^{N_{i-1}-1} f_{m,n}^{i-1} \cos\frac{\pi(2m+1)p}{2M_{i-1}} \cos\frac{\pi(2n+1)q}{2N_{i-1}} \quad (3)$$

for a block size of 8×8, $i = 0 \cdots 3$, $M_i = N_i = \frac{8}{2^i}$, $0 \le p \le M_i - 1$, $0 \le q \le N_i - 1$ and $a_0 = 1/\sqrt{M_s}$, $a_{1 \ldots M_i} = \sqrt{2/M_i}$.

For a 8×8 MB at base level 0, the DCT coefficients of the layers 0 to 3 are defined in terms of the base layer DCT coefficients as:

Pyramid base layer 0 MB is raw image $f_{p,q}^{0}$ p=0:7, q=0:7.

Pyramid layer 1 extracted from the base layer 0:

$$f_{p,q}^{1} = IDCT2\left(DCT2\left(f_{p,q}^{0}\right)\right) \quad p=0:3, q=0:3 \quad (4)$$

Pyramid layer 2 coefficients extracted from the layer 1:

$$f_{p,q}^{2} = IDCT2\left(DCT2\left(f_{p,q}^{1}\right)\right) \quad p=0:1, q=0:1$$

Pyramid layer 3, the apex coefficients extracted from layer 2:

$$f_{p,q}^{3} = IDCT2\left(DCT2\left(f_{p,q}^{2}\right)\right) \quad p=0, q=0$$

Note that, as shown in Fig. 1, the down-sampling by a factor of two is performed by simply retaining a quarter of the low-frequency index coefficients, the LL quadrant, and discarding the remaining three quarters, higher index, coefficients. As above, a set of similar equations can be defined for discrete wavelet transforms.

During the re-construction stages, starting from the apex of the multi-scale pyramid, image up-sampling by a factor of two is performed by a combination of a process of zero-padding of the 2D-DCT/DWT coefficients and the subsequent application of inverse 2D-DCT/DWT.

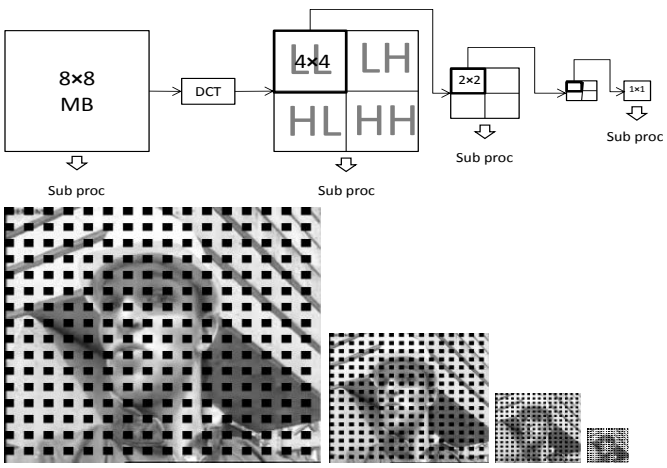

Fig. 1. Block diagram of a three-stage DCT pyramid image decomposition and its application to Foreman image. Down-sampled sub-images are extracted from LL quadrant of DCTs.

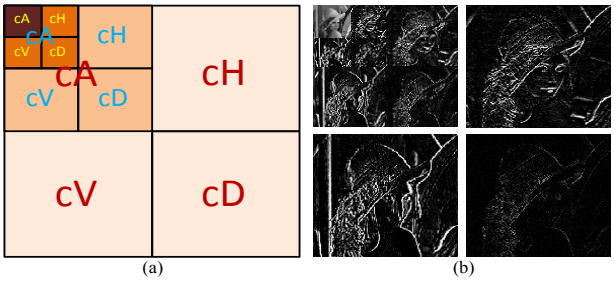

Fig. 2. (a) block diagram of the three-stage DWT pyramid image decomposition and its application to Lena image. Equivalence: cA=LL, cH=LH, cV=HL, cD=HH.

B. *Image Gap Concealment Using Pyramid Transform*

The proposed method for MB gap restoration, illustrated in Fig. 3, (Fig. 4 shows the subjective result) is as follows:

1) Decompose image macro-blocks into a DCT/DWT pyramid structure, with the apex of the pyramid representing the last stage where each MB of size 8×8 is reduced to one pixel only.
2) Starting from the pyramid apex interpolate the decimated gap using the local edge information from neighbouring pixels.
3) Using an edge detector, track the global edges in the interpolated images and produce edge skeleton layer.
4) Enhance the interpolated gap estimates using the global edge information.
5) Up-sample the enhanced interpolated image, via zero-padded inverse transform, and combine/merge with the available received samples of the same layer of up-sampling.
6) Go to step (2) and repeat the process for each intermediate stage of up-sampling.

The details of these sub-processes are described next.

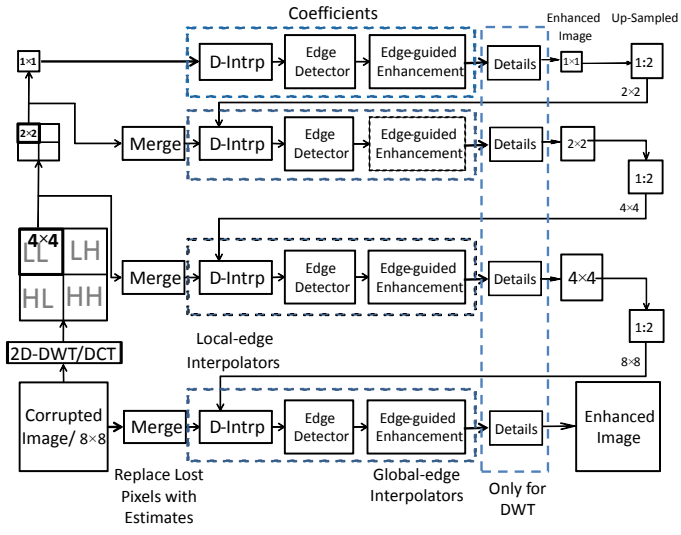

Fig. 3. Three-stage DCT/DWT pyramid image decomposition, (D-Interp=Directional Interpolation). Top row is pyramid apex, bottom row is the raw corrupted/enhanced image (details: three coefficient parts).

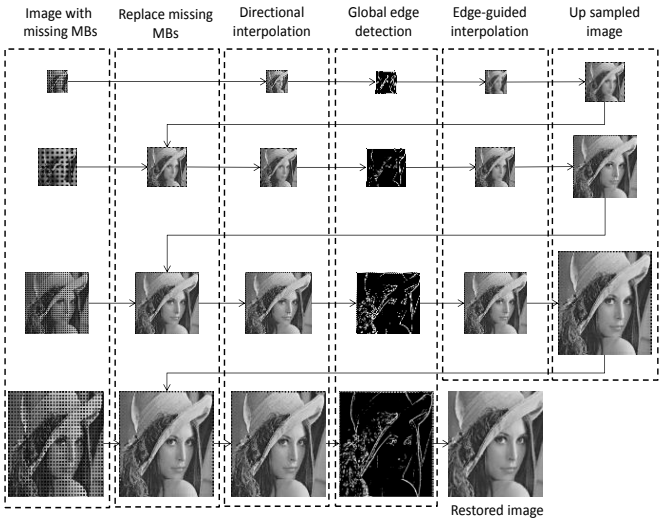

Fig. 4. Application of the proposed pyramid method to restoration of corrupted image of Lena with 25% of 8×8 block loss. Left top corner is the pyramid apex. Each row represents a layer which is up-sampled at the point of reentry to the next lower layer.

C. *Local Edge-Guided Image Gap Interpolation*

The proposed multi-scale gap restoration method preserve the local edge or texture information at each scale of the reconstruction process. Therefore, applying the edge based enhancement prevents the blurring distortions of textures and provides improved interpolation at a local texture level and in particular at the boundaries of the available and the missing samples. Note that the local edges may not show up at the later stage of detection of the global main edges after thresholding out the insignificant edges.

The main advantage of inclusion of local edge or texture within pyramid image restoration is that global edge detection would be erroneous without first interpolating the gaps with a local texture interpolator as an initial approximation. Hence, the benefits of local texture interpolation are:

1) Interpolation of textures within segmented homogenous regions;
2) Pre-processing for subsequent edge-guided interpolation across 'global' segments;
3) Can be used in strategies that combined local and global interpolations.

At each multi-scale level, spatial gap concealment interpolates the missing block by using the edge information obtained from the surrounding neighbours. Preserving the texture edges is important for successful error concealment. In this respect several observations are instructive:

1) Along the direction of an edge, the differences of pixel values are relatively small;
2) Across the direction of an edge the differences of pixel values are relatively large;
3) On either side of a gap, the differences of pixel values across an edge are consistent and of similar sign, with the possible exception of the gap coinciding with the end-points of an edge segment.

The estimate for the missing pixel at the final level of decomposition, i.e. at the pyramid apex, is an edge-weighted mean of the neighbouring pixels with consistent edges. At the successive levels where an $M \times M$ block replaces a gap, directional edge-guided interpolation are used to fit the missing blocks with the edge patterns of the available neighbouring pixels.

As illustrated in Fig. 5, the directional interpolation preserves the following three types of local edges:

1) Horizontal edges above and below the missing pixels, Fig. 5.a.
2) Vertical edges to the left and right of the missing pixels, Fig. 5.b.
3) Cross edges across four directions, Fig. 5.c.

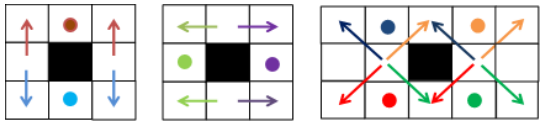

(a) (b) (c)

Fig. 5. Local-edge guided directional interpolation for each missing pixel at the apex of multi-scale pyramid (in eight possible directions). Black pixels represent the missing pixel. The direction of edge at each surrounding pixel (shown by dot circles) is computed by using the information of surrounding pixels shown by two arrows with the same colour.

At the apex of the pyramid, where an MB is reduced to one pixel, the edge-enhanced estimation of the missing sample is given by the following expression.

$$f_{m,n} = \sum_{H,V,C \in RI} \sum_{k,l} w_{m+k,n+l}\left(f_{m+k,n+l} + E_{m+k,n+l}\right) \qquad (5)$$

where E=edge and $E(m+k, n+l)$ is a local estimation of the edge obtained separately in each of horizontal (H), vertical (V) and cross directions (C) depicted in Fig. 5 and RI is the Region of Interest which for local interpolation, on un-segmented image, includes information from all neighbouring pixels. The edges along the directions $(m,n) \rightarrow (m+k, n+l)$ are obtained from the average of all the available edges of the same direction in the immediate neighbourhood of the missing sample. For example, at the apex level, where the gap is reduced to one sample, for the horizontal direction (Brown dot and corresponding brown arrows which represent the direction and neighbouring pixels, respectively), $E(m-1, n)$, may be obtained as:

$$E_{m-1,n} = \begin{cases} 0 \;\; if \; E_{m-1,n-1} \times E_{m-1,n+1} < 0 \\ 0.5\left(E_{m-1,n-1} + E_{m-1,n+1}\right) \;\; else \end{cases} \qquad (6)$$

As can be seen in Equation 6, if both estimates of edges for $E_{m-1,n-1}$ and $E_{m-1,n+1}$ are not in the same direction, the value of $E_{m-1,n}$, is set to zero, otherwise $E_{m-1,n}$ is set to the average value of the estimates. In order to make an estimate consistent with the most distinct neighbourhood edges, the edge combination weights can be expressed as a function of the intensity of the edges, as:

$$w_{m+k,n+l} = \frac{E_{m+k,n+l}}{\sum_{k=-1:1, l=-1:1 \; k,l \neq 0} E_{m+k,n+l}} \qquad (7)$$

Note that $\sum_{k=-1:1, l=-1:1 \; k,l \neq 0} w_{m+k,n+l} = 1$.

After interpolation of the apex sample, at the subsequent stages of interpolation, for blocks of size 2×2, 4×4 and 8×8 a strategy similar to that described above is used. Staring from the outer boundaries of the MB, the missing pixels are progressively replaced towards the center, using, the edge-guided interpolation, for an estimate consistent with the neighbouring edges in each of the horizontal, vertical and cross directions.

D. Global Edge-Guided Image Gap Interpolation

From the literature it is observed that preserving the *local* edges mitigates blurring distortions of textures and provides improved interpolation at a local texture level and in particular at the boundaries of the available and the missing samples. For further improvement where the missing blocks contain significant edges, the *global* edge information, not necessarily evident within the lost macro-blocks, need to be utilised.

The global edges are used in a manner as to avoid blurred/smeared interpolation across the significant edges; the main cause of large interpolation errors and visible distortions. Hence with the availability of the boundary traces of the edges, it is possible to segment the pixels within and in the neighborhood of missing blocks and to confine the available samples used for interpolation of a missing sample to within a relatively homogeneous region on each side of the edge or onto the edge itself as required.

After edge-based segmentation, the interpolation Equation 5 will have its regions of interests (RI), for estimation of the edges, $H, V, C \in RI$, confined to edge-segmented regions composed of relatively homogenous textures.

Note from Fig. 3 that the global edge-guided interpolation is performed after local edge interpolation in order to mitigate the impact of the missing samples on the edge detection. For estimation of the main edges in the image, we investigated the application of a popular edge detection method namely the Canny edge detector.

D.2 Canny Edge Detector

Canny detector is a multi-stage algorithm for detection and tracing of the edges in images. The variance of the Gaussian filter and the maximum and minimum thresholds of the significant edges can be varied to change the sensitivity of the Canny detector. Fig. 6 shows the application of a Canny detector to multi-scale Lena and Pepper with image scale progressively down sampled by 2:1, in three stages, from size 512×512 to 64×64.

Fig. 6. Canny edge detector output for multi-scale Lena and Peppers at scales from left to right: (a) 512^2, (b) 256^2, (c) 128^2, (d) 64^2.

Incorporating Global Edge-guided Interpolation in an Iterative Loop

At the base level of the process, an iterative pruning strategy is applied for edge detection. This relies on varying the two parameters of a Canny detector, the variance of the Gaussian filter and the threshold of the significant edges, at each iteration in order to achieve improved results. As shown in Fig. 8, the experiment starts the process by using a higher level of Canny edge details at the first iteration, and then reduces the amount of details. Simulation results, Fig. 7, show the overall PSNR obtained by fixing the Gaussian filter variance at an empirically obtained optimal value and then varying the threshold in the range 0.01-0.05. Note that starting from a thresh value of 0.01 the best PSNR is obtained at the 4^{th} iteration after three discrete -step increase in the threshold value (therefore, the number of iteration set to four).

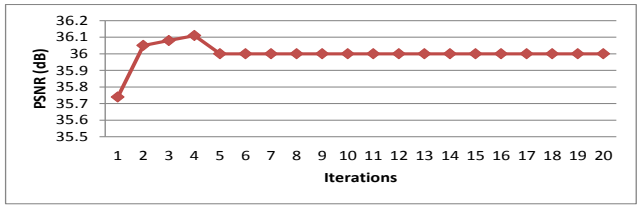

Fig. 7. Performance variation with increasing threshold in the range 0.01-0.05 for a loss rate of 25% on Lena for the last stage of image reconstruction.

Fig. 8. Lena edge layers, from the left to right, four stages of iteration for increasing values of threshold.

III. EXPERIMENTAL RESULTS

For performance evaluation results the proposed algorithm has been tested on a number of standard test images namely; Lena, Peppers, Man, Boat, Elaine and Baboon. The image sizes are 512×512 pixels, with each grey-scale or one of the primary colours represented by 8 bits per pixel in unsigned integer format with a range of 0-255. The size of the missing macro-blocks is set to 8×8 and 16×16 pixels. Three types of missing MBs are evaluated; regular missing MB ≈ 25% loss rate, (Fig. 9 and Fig. 10), random 8×8 missing MB ≈ 10% loss rate (Fig. 12), ≈ 25% and ≈ 40% loss rate (Fig. 11), regular and random 16×16 missing MB (Fig. 13, Fig. 14). The choice of the percentage loss is guided by our desire to compare our results with available seventeen results reported in the literature [7,23,28,30]. The PSNR results of restored images are given in Tables I–VI. As can be observed from the tables, the proposed EC algorithm achieves the best performance for all types of loss.

The performance measure criteria used for assessment of the quality of image recovery is the widely employed Peak-Signal-to-Noise-Ratio (PSNR) defined as:

$$PSNR = 20 \log_{10} \frac{MAX_I}{RMSE} \quad \text{dB} \qquad (8)$$

where $MAX_I = 255$ for a pixel value represented in unsigned integer format and the root mean squared error (RMSE) function is defined as:

$$RMSE = \sqrt{\frac{1}{N}\sum_{domain}(f(m,n) - fr(m,n))^2} \qquad (9)$$

where f and fr are the clean test image and restored image respectively and the domain over which the RMSE is calculated may include only the missing samples or it may alternatively include the entire image samples composed of the missing and the available samples and N is the total number of samples used in calculation of the RMSE.

A. *Evaluation Case 1- Image with Regular Missing MBs*

The proposed method is applied to images of Lena, Man peppers, Boat and Elaine. The PSNR results are compared to a set of published work in total representing a number of methods that employ Bayesian and/or edge information for the recovery of regular lost macro-blocks. The results are displayed in three different tables. Table I and Table II represents comparison with published results, where the PSNR are averaged over the whole image including the available samples and Table III represents comparison with published results where the PSNR are averaged over the missing pixels only.

Table I illustrates the performance of the several methods (values are taken from [30]). As displayed in Table I, the proposed method performs better than the alternatives considered and there is an improvement of 0.79 in DCT case and 0.85 dB in DWT case to compare with the best average performance when the PSNR are computed from whole image. In addition, in Table II (values are taken from [23]) fourteen well-known published works are compared with the proposed method. The proposed method's outcomes remarkably surpass the best result among them by 0.36 dB. Table III (values are taken from [7,28]) includes results between six published techniques and the proposed method on Lena, and there is an increase of 1.27 dB and 1.32 dB for DCT and DWT respectively, compared with the best result among all methods.

To better represent the improved performance of the proposed method subjective quality comparisons are given in Figs. 9–10. Fig. 9. illustrates the performance comparison between the proposed method and six classical published works on the Man image.

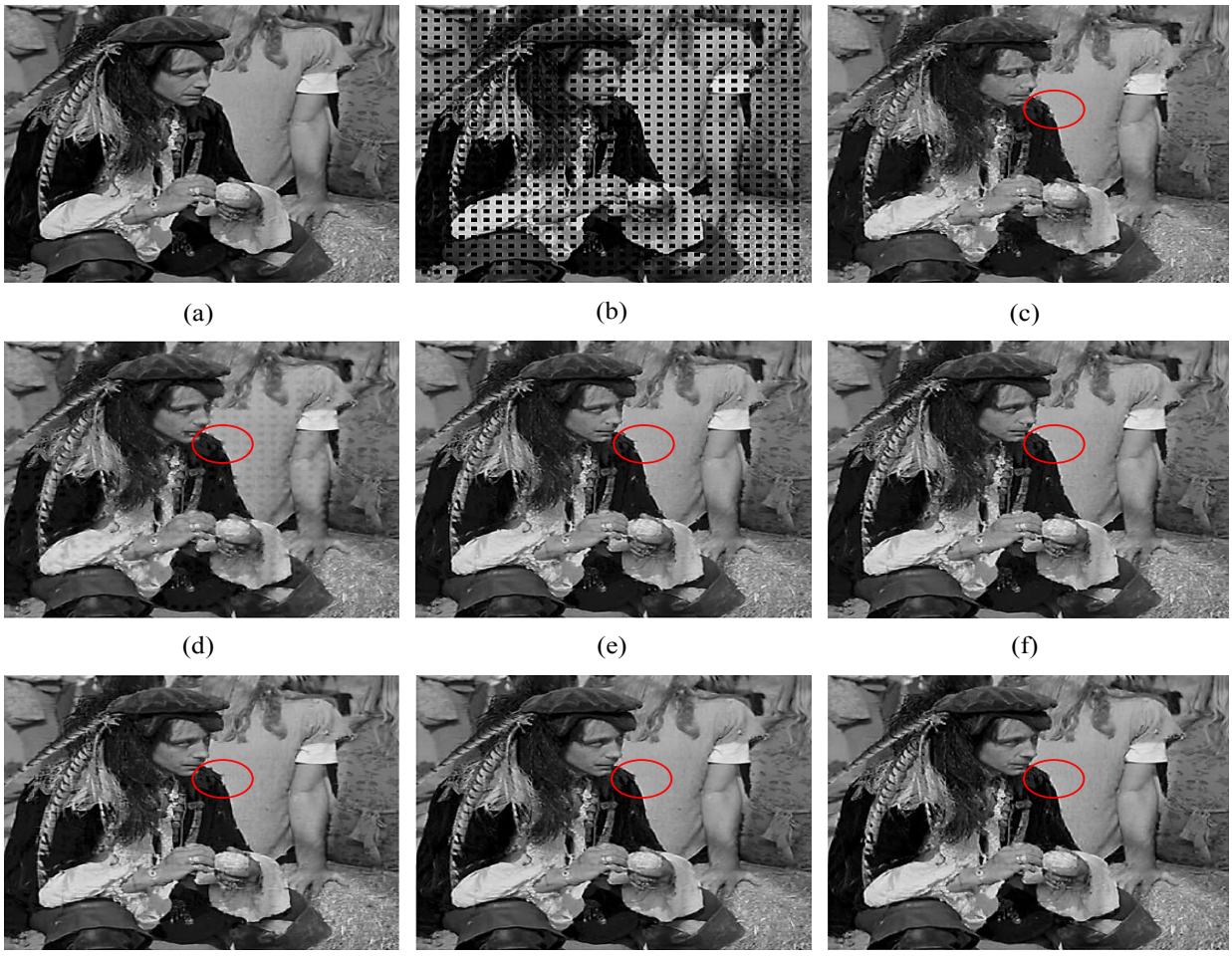

Fig. 9. Experiment on block size of 8×8 pixels of the "Man" image. (a) Original 512×512, (b) damaged image with 25% missing blocks. Restoration using the methods of :(c) [35] (PSNR = 25:47 dB), (d) [29] (PS PSNR = 27:25 dB), (e) [37] (PSNR = 27:65 dB), (f) [36] (PSNR = 27:44 dB), (g) [21] (PSNR = 27:94 dB), (h) [30] (PSNR = 29:87 dB), (I) Proposed method (31.61 dB).

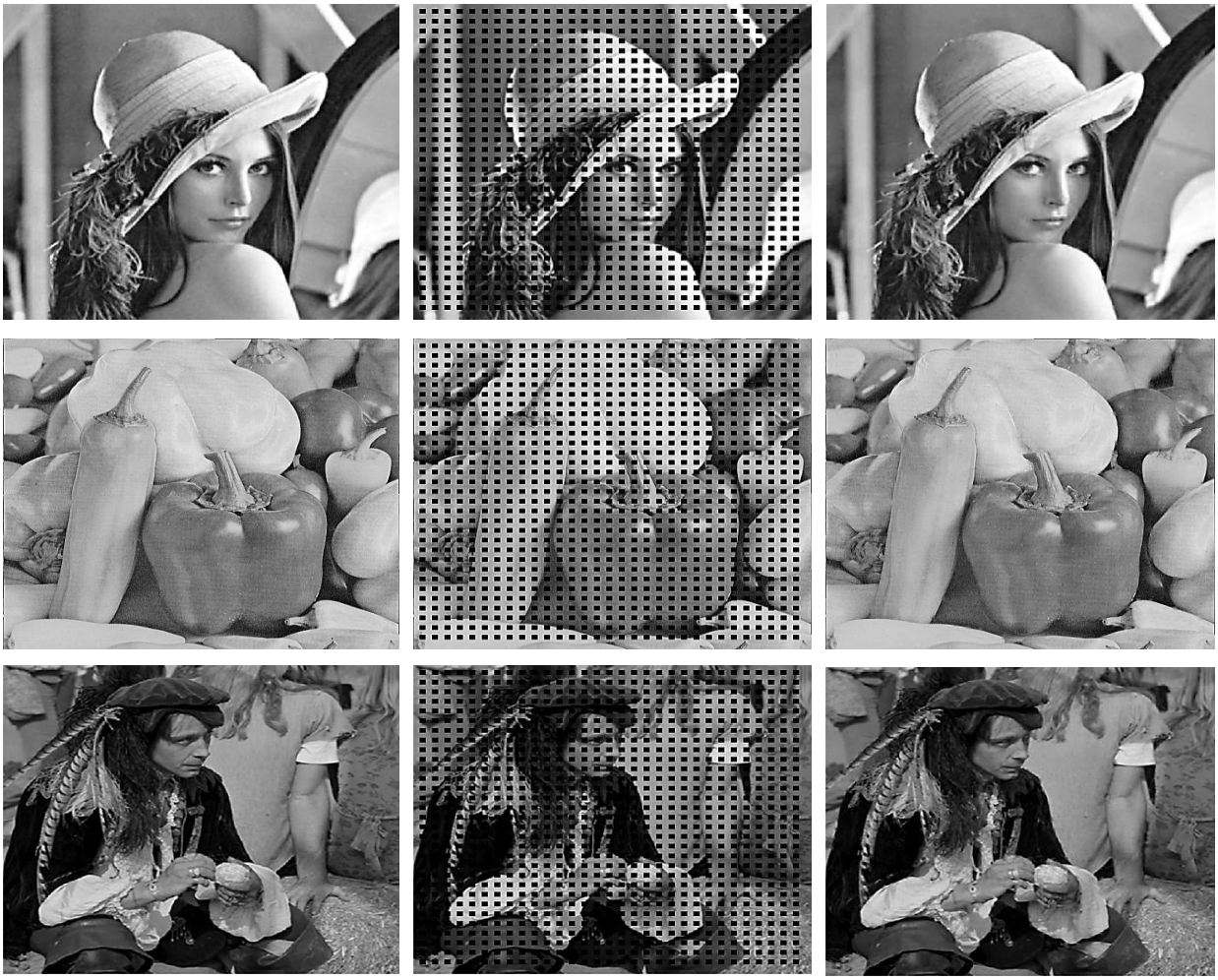

Fig. 10. From left to right; the original images, the image with 25% regular pattern loss and the restored images for Lena, Pepper and Man.

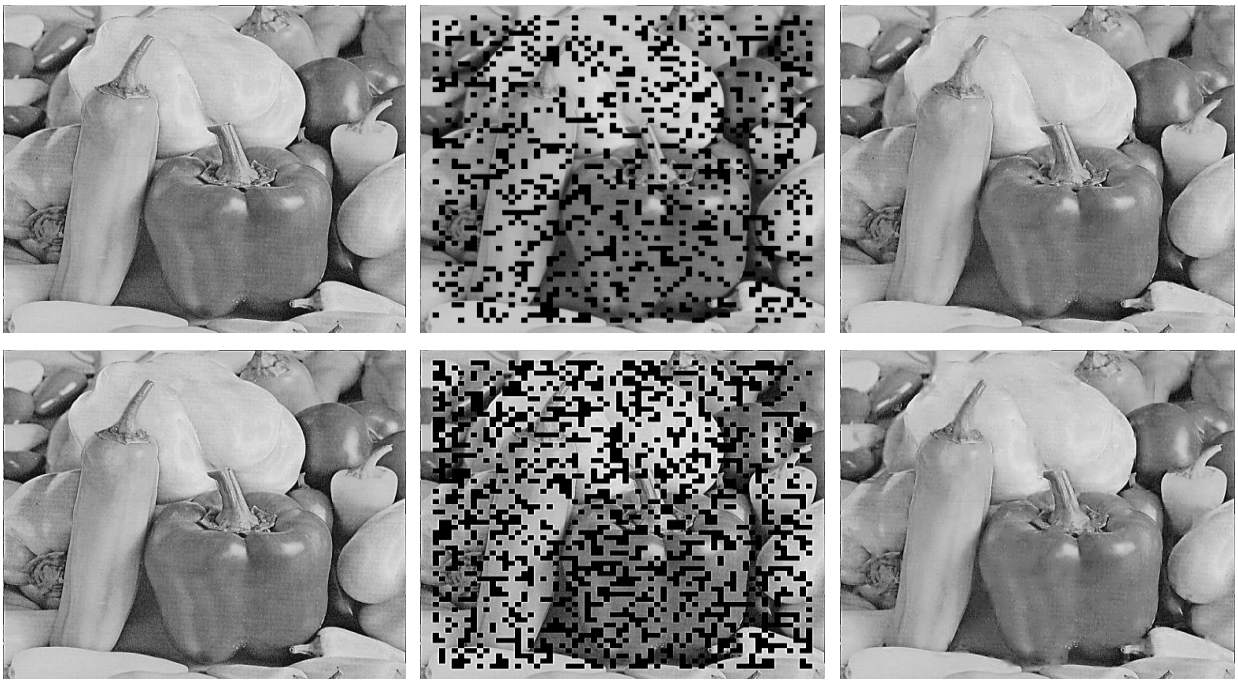

Fig.11. Top from left to right; the original Peppers image, the image with 25% random loss and the restored image, bottom the original Peppers, the image with 40% random loss with PSNR of 33.84 dB and 30.95 dB respectively, and the restored image.

Fig. 12. From left to right; the original Lena, Man and Elain images, the image with 10% random loss and the restored image.

Table I
Performance comparisons for regular pattern loss rate 25%, MB size= 8×8, PSNR calculated over whole image on Lena: proposed 1, with the DCT. Proposed 2, the DWT.

Methods	**PSNR (dB)**					
	Lena	***Man***	***Pepper***	***Boat***	***Elaine***	***Ave.***
[35]	28.68	25.47	27.92	26.33	29.84	27.65
[29]	29.99	27.25	29.97	27.36	30.95	29.10
[36]	31.69	27.44	31.72	29.22	32.10	30.43
[37]	31.86	27.65	31.83	29.36	32.07	30.55
[21]	31.57	27.94	32.76	30.11	31.92	30.86
[30]	34.65	29.87	34.20	30.78	34.63	32.83
[11]	34.91	30.62	35.18	31.40	35.63	33.55
Proposed DCT	36.08	31.59	36.23	31.76	36.08	34.34
Proposed DWT	**36.12**	**31.61**	**36.35**	**31.79**	**36.13**	**34.40**

Table II
Performance comparisons for MB loss rate of 25%, MB size= 8×8, PSNR calculated over whole image for Lena.

Methods	**Image Lena**	**Methods**	**Image Lena**
	PSNR (dB)		**PSNR (dB)**
[29]	29.99	[30]	34.65
[35]	28.68	[39]	34.45
[36]	31.69	[11]	34.91
[37]	31.86	[24]	34.07
[21]	31.57	[23]	35.70
[40]	32.05	[27]	33.74
[28]	35.70	[38]	34.79
Proposed DCT	36.08		
Proposed DWT	**36.12**		

Severe blocking artifacts are observed (Fig. 9) using [35], [29], and [37]. Although the blocking artifacts are smaller in [36], [21] and [30], they produce blurred and lumpy boundaries, as shown around the shoulder of Man. Furthermore, the outcomes show that the proposed method improved the PSNR result by 1.74 dB when compared with the best performance among all the other methods. Moreover, Fig. 10 demonstrates the original, erroneous and reconstructed images after applying the proposed error concealment method and it can be seen that the result is not blurry, with the shape having been recovered correctly. In addition, Fig. 13 illustrates the performance comparison between the proposed method and three previously published methods for 16×16 missing block size on Lena, and the proposed method performs better.

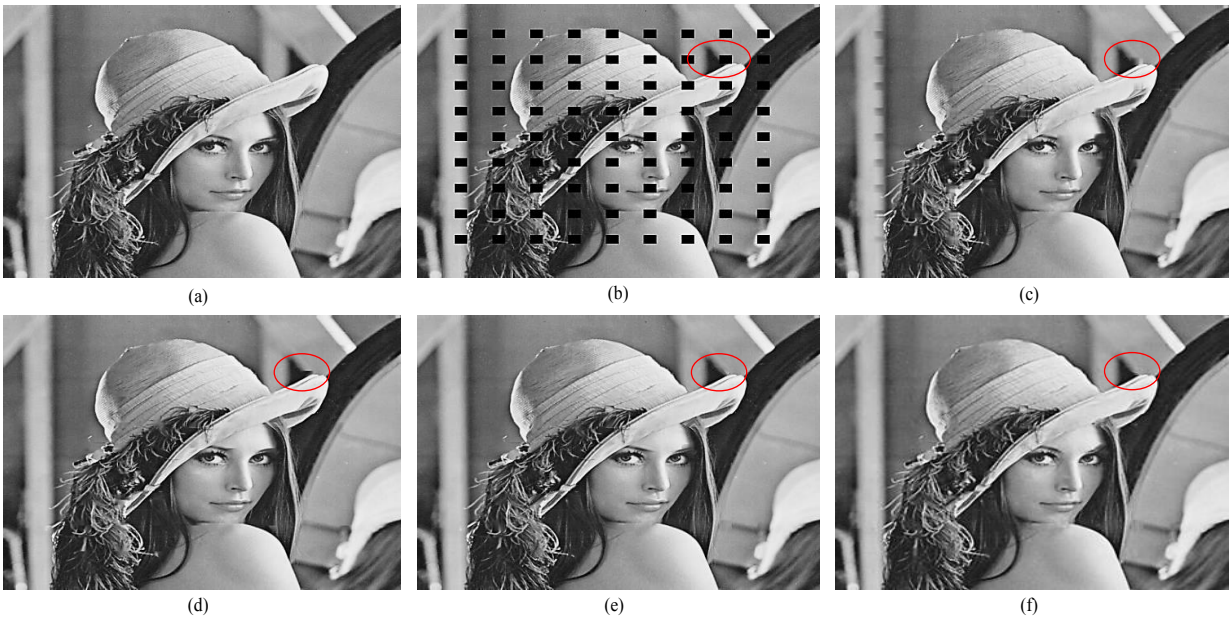

Fig. 13. Experiment on block size of 16×16 pixels of the Lena image. (a) Original image 512×512, (b) damaged image blocks. Restoration using the methods of: (c) [41] (PSNR = 33.62 dB), (d) [28] (PSNR = 37.48 dB), (e) [11] (PSNR = 37.37 dB), (f) Proposed DWT (PSNR = 37.65 dB).

Table III
Performance comparisons for regular loss rate 25% MB size= 8×8, PSNR calculated just for region of missing block on Lena: proposed 1, with the DCT. Proposed 2, the DWT.

Methods	**Image Lena**
	PSNR (dB)
[7]	28.51
[10]	22.97
[30]	26.00
[39]	28.11
[27]	27.43
[28]	28.25
Proposed DCT	29.78
Proposed DWT	**29.83**

B. Evaluation Case 2 – Image with Random Missing MBs

The random loss pattern involves missing macro-blocks at random position that may include a random sequence of adjacent horizontal and/or vertical losses. Therefore, in the random model of packet loss there is no specific pattern of loss and two or more lost MBs could be adjacent. As the positions of the missing macro-blocks are random and distinct in each evaluation test and therefore, the program is applied for a number of iterations to find the mean PSNR distortion.

Table IV
Performance comparisons for random loss rate of 10% (MB size = 8×8) on Lena rerun five times (DWT).

Image / **Result**	**Lena**					
	1	**2**	**3**	**4**	**5**	**AVG.**
PSNR (dB)	39.11	39.06	39.35	38.73	39.58	**39.16**

Table IV shows the number of iterations and the average of those results on Lena (the same process are done for each image to find the mean PSNR distortion).Table V shows the proposed approach performs better than the rest for random MB loss rate of size (8×8), and there is an improvement of 0.16 dB (in DCT case) compared with the best average performance among all results, and also there is an improvement of 0.25 dB (in DWT case) compared with the best average performance among all results. The `performance of the algorithm is tested in case of 16 × 16 block loss, and Table VI (values taken from [23]) shows the results on Lena, Baboon and Elain. The average gain over the best performance along all published works is over 0.29 dB and 0.40 dB in DCT and DWT cases, respectively.

Table V
Performance comparisons for MB loss rate random 10%, MB size= 8×8, PSNR calculated over whole image for Lena, Man and Elain.

Methods	**PSNR (dB)**			
	Lena	***Man***	***Elain***	***AVG.***
[29]	32.32	32.17	34.20	32.89
[40]	35.06	34.40	36.79	35.41
[39]	35.09	33.95	36.73	35.25
[24]	35.11	34.14	36.38	35.21
[27]	36.82	34.63	38.48	36.64
[38]	37.54	35.82	39.16	37.50
[36]	37.84	35.70	39.44	37.66
[28]	38.58	35.59	39.73	37.96
[23]	38.63	36.36	40.03	38.34
Proposed DCT	39.08	36.32	40.11	38.50
Proposed DWT	**39.16**	**36.42**	**40.21**	**38.59**

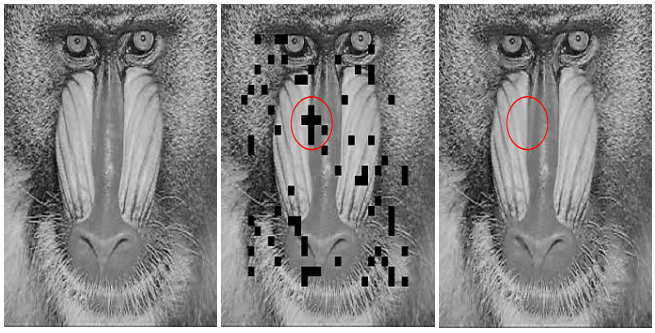

Fig. 14. From left to right; the original images, the image with random consecutive 16 × 16 MB loss and the restored images for Baboon.

In order to evaluate the subjective performance result for the random block loss the application of the proposed method to Lena, Man and Elain images, are shown in Fig. 12. Moreover, Fig. 11 shows the results for 25% and 40% random missing blocks on the Peppers image. Even though many missing blocks are included in each process, the proposed method is able to reconstruct the edges and texture within the image Furthermore, random block loss of 16 × 16 is tested on Baboon image (Fig. 14). It clearly shows that the proposed algorithm completely recovers the boundaries along with the texture. Fig. 15 demonstrates the performance of the proposed method in the case of various random loss rates of 10%, 25% and 40% for Lena, Man, and Elain images. Fig. 15 shows that the average amount of the proposed method surpassed the average of the best published method. It is been observed that by increasing the loss rate the performance decreased, but it is still convincing.

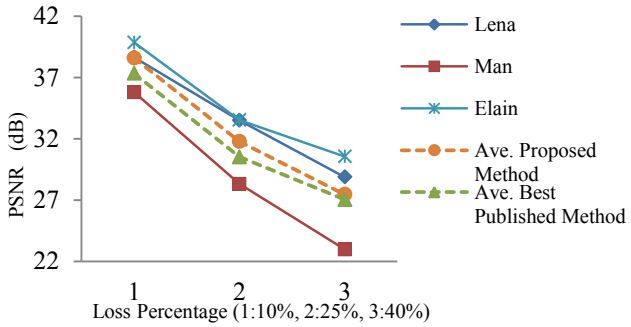

Fig. 15. The performance (PSNR) of the proposed method in the case of various random loss rate (10%, 25%, 40%) for Lena, Man and Elain images.

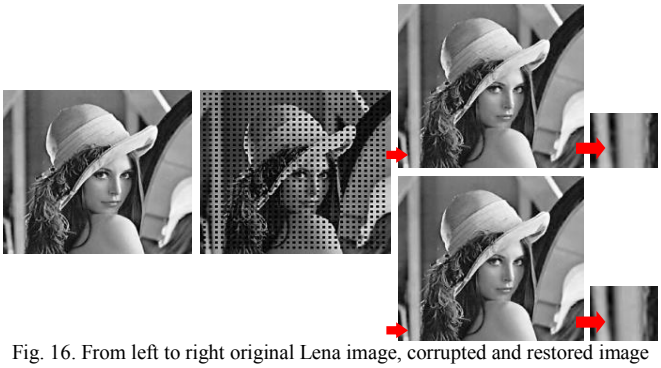

Fig. 16. From left to right original Lena image, corrupted and restored image with DCT top and DWT down.

Table VI
Performance comparisons for MB loss rate random size= 16×16, PSNR calculated over whole image for Lena, Baboon and Elain.

Methods	PSNR (dB)			
	Lena	***Baboon***	***Elain***	***AVG.***
[29]	31.68	30.26	32.27	31.40
[40]	34.75	30.95	34.88	33.52
[39]	35.17	31.06	34.11	33.44
[24]	34.66	29.88	33.63	32.72
[27]	37.87	30.31	36.89	35.02
[38]	38.57	31.72	36.64	35.64
[36]	37.24	31.73	36.36	35.11
[28]	38.44	30.74	37.33	35.50
[23]	**39.15**	31.91	**37.93**	36.33
Proposed DCT	38.54	33.56	37.78	36.62
Proposed DWT	38.62	**33.68**	37.91	**36.73**

Run-Time Comparison

To compare the run time of different EC algorithms, test 512×512 images (*Lena*, *Baboon* and *Elaine*) are tested. The averaged run time for different loss pattern is presented in Table VII. The computation time reported in the table is obtained with non-optimized MATLAB implementations with Intel CORE i5, 2.3 GHz CPU and 4 GB memory.2 We can see that the proposed algorithm is much faster (especially in the proposed DCT method) than the recently proposed [23,27,28,38] algorithms. Although the proposed algorithm requires longer time than some methods, its advantages over other methods are obvious in terms of objective and subjective evaluations, as shown in previous Sections.

Table VII
Average run time in second comparison for 512×512 images, different MB loss rate for Lena, Baboon and Elain.

Methods	Run Time (second)		
	Regular 8×8	***Random 8×8***	***Random 16×16***
[29]	4.82	1.91	2.59
[40]	0.10	0.08	0.07
[39]	1.28	0.57	0.59
[24]	4.59	2.81	9.09
[27]	79.75	29.84	124.68
[38]	426.59	170.88	89.16
[36]	9.05	3.56	3.24
[28]	90.28	33.66	29.44
[23]	155.30	63.22	53.30
Proposed DCT	53.62	43.32	45.71
Proposed DWT	65.19	56.98	58.13

Fig. 16 shows there is a slight improvement of details in DWT, compared with DCT, but the run time is higher for DWT (Table VII) as it was expected from previous works [43].

IV. CONCLUDING REMARKS

In this paper we have proposed a method for restoration of lost macro-blocks in digital images. The proposed algorithm includes combination of multi-resolution transforms, directional interpolation and edge-guided enhancement capable of restoring missing blocks including the edges. The main contribution of this work is the incorporation of local and global edge-guided interpolators within a pyramid structure in an iterative loop at the last stage. Two types of pyramid transformation were evaluated namely DCT and wavelets. The methods were evaluated on a number of different test images in a range of loss rates for regular and random pattern of losses. The results for DCT and wavelets are similar (with a slight improvement of details in DWT) and achieve better performance than other state-of-the-art methods in terms of objective and subjective evaluation. The incorporation of local, global edges and iterative process improves interpolation. The results obtained from DCT pyramid are comparable with those obtained from wavelets with the DCT offering a slight advantage in computation time. The experimental results demonstrate that significant improvement in the quality and PSNR of the restored images are obtained by the proposed edge guided image restoration method. An interesting aspect of this work is the use of iterative methods for improving various layers of pyramid reconstruction including the image and the edge, or skeleton, layers. This is an area of research where further work may be fruitful. Moreover, to extend the proposed methodology it will apply into the colour and moving images.

REFERENCES

[1] K. Khoshelham and S. O. Elberink, "Accuracy and Resolution of Kinect Depth Data for Indoor Mapping Applications," *Journal of Sensors*., vol. 12, pp. 1437-1454, 2012.

[2] A. Prochazka, O . Vysata, and E. Jerhotova, "Wavelet Use for Reduction of Watershed Transform Over-Segmentation in Biomedical Image Processing," in *Proc*. *Int*. *Conf*. ITAB, pp. 1-4, 2010.

[3] Y. Wang and Q. Zhu, "Signal loss recovery in DCT-based image and video codecs," in *Proc*. *SPIE Vis*. *Commun*. *Image Process*. *Vis*.*Commun*., vol. 1605, pp. 667–678, 1991.

[4] M. Yang and N. G. Bourbakis, "An Efficient Packet Loss Recovery Methodology for Video Streaming Over IP Networks," *IEEE Trans*. *Broadcasting*, vol. 55, no. 2, Jun. 2009.

[5] M. Hayasaka, M. Gamage, and T. Miki, "An Efficient Loss Recovery Scheme for On-demand Video Streaming over the Internet," *IEEE*, pp. 1301 – 1306, 2005.

[6] M. Ira, "Polycom's Lost Packet Recovery (LPR) Capability," Polycom, Wainhouse Research, 2008.

[7] G. Zhai, X Yang, W. Lin, and W. Zhang, "Bayesian Error Concealment with DCT Pyramid for Images," *IEEE Trans*. *Circuits and Systems for video technology*, vol. 20, no. 9, Sept. 2010.

[8] H. Asheri, H. R. Rabiee, N. Pourdamghani, and M. Ghanbari, "Multi-Directional Spatial Error Concealment Using Adaptive Edge Thresholding," *IEEE Trans*. *Consumer Electronics*, vol. 58, no. 3, Aug. 2012.

[9] Y. Wang and Q. F. Zhu, "Error control and concealment for video communication: A review," *Proceedings of the IEEE*, vol. 86, no. 5, pp. 974-997, 1998.

[10] D. Agrafiotis, D. R. Bull, and C. N. Canagarajah, "Enhanced Error Concealment With Mode Selection," *IEEE Trans*. *Circuits and Systems for video technology*, vol. 16, no. 8, Aug. 2006.

[11] W. Kim, J. Koo, and J. Jeong, "Fine Directional Interpolation for Spatial Error Concealment," *IEEE Trans*. *Consumer Electronics*, vol. 52, no. 3, Aug. 2006.

[12] Y.K. Wang, M. M. Hannuksela, V. Varsa, A. Hourunranta, and M. Gabbouj, "The error concealment feature in the H.26L test model," in Proc. ICIP, pp. 729–73, 2002.

[13] S.-C. Hsia, "An edge-oriented spatial interpolation for consecutive block error concealment," *IEEE Signal Process*. *Lett*., vol. 11, no. 6, pp. 577–580, Jun. 2004.

[14] J.W. Suh, and Y.S. Ho, "Error concealment based on directional interpolation," *IEEE Trans*. *Consum*. *Electron*., vol. 43, no. 3, pp. 295–302, Aug. 1997.

[15] W. Kwok and H. Sun, "Multidirectional interpolation for spatial error concealment," IEEE Trans. Consum. Electron., vol. 39, no. 3, pp. 455–460, Aug. 1993.

[16] Z. Wang, Y. Yu, and D. Zhang, "Best neighborhood matching: An information loss restoration technique for block-based image coding systems," *IEEE Trans*. *Image Process*., vol. 7, no. 7, pp. 1056–1061, Jul.1998.

[17] K. Meisinger, and A.Kaup, "Spesial error concealment of corrupted image data using frequency selectiv extrapolation," in *Proc*. *Int*. *Conf*. *Acoust*., *Speech, Signal Process*. *(ICASSP)*, pp. 209-212, 2004.

[18] A. Kaup, K. Meisinger, and T. Aach, "Frequency selective signal extrapolation with applications to error concealment in image communication," *AEU-International Journal of electronics and communication*,. vol. 59, no. 3, pp. 147–156, Jun. 2005.

[19] S. Padmavathi, B. Priyalakshmi, and K.P. Soman, "Hierarchical Digital Image Inpainting Using Wavelets," *Signal & Image Processing: An International Journal (SIPIJ)*, vol. 3, no. 4, 2012..

[20] Y. Wang, Q.-F. Zhu, and L. Shaw, "Maximally smooth image recovery in transform coding," *IEEE Trans*. *Commun*., vol. 41, no. 10, pp. 1544–1551, Oct. 1993.

[21] Z. Alkachouh, and M. G. Bellanger, "Fast DCT based spatial domain interpolation of blocks in images," *IEEE Trans*. *Image Process*., vol. 9, no. 4, pp. 729–732, Apr. 2000.

[22] G. Zhai, and X. Yang, "Image reconstruction from random samples with multiscale hybrid parametric and nonparametric modeling," *IEEE Transactions on Circuits and Systems for Video Technology*; pp. 22(11):1554-632012.

[23] J. Liu, G. Zhai, X. Yang, B. Yang, and L. Chen, "Spatial Error Concealment With an Adaptive Linear Predictor," *IEEE Transactions on Circuits and Systems for Video Technology*, vol. 25, no. 3, pp. 353-366, 2015.

[24] Z. Rongfu, Z. Yuanhua, and H. Xiaodong, "Content-adaptive spatial error concealment for video communication," *IEEE Trans*. *Consum*. *Electron*., vol. 50, no. 1, pp. 335–341, Jan.

[25] D.Tschumperle, and R.Deriche, "Vector-Valued Image Regularization with PDEs: A Common Framework for Different Applications," *IEEE Trans*. vol. 27, no. 4, Apr. 2005.

[26] F. Marvasti, A. Amini, F. Haddadi, M. Soltanolkotabi, B. H. Khalaj, A. Aldroubi, S. Holm, S. Sanei, and J. Chambers, "A Unified Approach to Sparse Signal Processing," Feb. 2009.

[27] J. Koloda, J. Ostergaard, S.H. Jensen, V. Sanchez, and A.M. Peinado, "Sequential Error Concealment for Video/Images by Sparse Linear Prediction", *Multimedia, IEEE Transactions on*, vol. 15, no. 4, pp. 957-969, 2013.

[28] X. Li, and M. T. Orchard, "Novel Sequential Error-Concealment Techniques Using Orientation Adaptive Interpolation," *IEEE Trans*. *Circuits Syst*. *Video Technol*., vol. 12, no. 10, Oct. 2002.

[29] H. Sun, and W. Kwok, "Concealment of damaged block transform coded images using projection onto convex set," *IEEE Trans*. *Image Process*., vol. 4, no. 4, pp. 470–477, Apr. 1995.

[30] J. Park, D.-C. Park, R. J. Marks, and M. A. El-Sharkawi, "Recovery of image blocks using the method of alternating projections," *IEEE Trans*. *Image Process*., vol. 14, no. 4, pp. 461 – 474, Apr. 2005.

[31] Kyung-Su Kim, Hae-Yeoun Lee, and Heung-Kyu Lee, "Spatial Error Concealment Technique for Losslessly Compressed Images Using Data Hiding in Error-Prone Channels," *Journal of Communication and Networks*, vol. 12, no. 2, Apr. 2010.

[32] W. Zeng and B. Liu, "Geometric-structure-based directional filtering for error concealment in image/video transmission," in *Proc. SPIE Conf. Wireless Data Transmission*, vol. 2601, pp. 145–156, 1995.

[33] Q.-F. Zhu, Y. Wang, and L. Shaw, "Coding and cell loss recovery for DCT-based packet video," *IEEE Trans. Circuits Syst. Video Technol.*,vol. 3, no. 3, pp. 248–258, Jun. 1993.

[34] J. Park, D.C. Park, R. J. Marks, and M. A. El-Sharkawi, "Block loss recovery in DCT image encoding using POCS," in *Proc. Int. Symp.Circuits Syst. (ISCAS)*, pp. 245–248, May. 2002.

[35] M. Ancis, and D.D. Giusto, "Reconstruction of missing blocks in JPEG picture transmission," *Communications, Computers and Signal Processing, IEEE Pacific Rim Conference on*, pp. 288, 1999.

[36] S. Shirani, F. Kossentini, and R. Ward, "Reconstruction of baseline JPEG coded images in error prone environments," *Image Processing, IEEE Transactions on*, vol. 9, no. 7, pp. 1292-1299, 2000.

[37] S.S. Hemami, and T.H. Meng, "Transform coded image reconstruction exploiting interblock correlation," *Image Processing, IEEE Transactions on*, vol. 4, no. 7, pp. 1023-1027, 1995.

[38] J. Koloda, V. Sánchez, and A. M. Peinado, "Spatial error concealment based on edge visual clearness for image/video communication," *Circuits, Syst., Signal Process.*, vol. 32, no. 2, pp. 815–824, Apr. 2013.

[39] G. Zhai, J. Cai, W. Lin, X. Yang, and W. Zhang, "Image error-concealment via Block-based Bilateral Filtering," *Multimedia and Expo, IEEE International Conference on*, pp. 621, 2008.

[40] V. Varsa, M.M. Hannuksela, and Y.K. Wang, "Non-normative error concealment algorithms", *ITU-T VCEG-N62*, 2001.

[41] P. Salama, N. B. Shroff, and E. J. Delp, "Error concealment in encoded video streams," *Signal Recovery Techniques for Image and VideoCompression and Transmission*, pp. 199-233, 1998.

[42] B. Langari, S. Vaseghi, and Seyed Kamran Pedram, "Multi-resolution edge-guided image gap restoration," *Signal Processing and Information Technology(ISSPIT), IEEE International Symposium on*, pp. 000374-000379, 2013.

[43] A. Katharotiya, S. Patel, and Mahesh Goyani, "Cpmparetive Analysys between DCT and DWT Techniques of Image Comparession," *Journal of Information Engineering and Applications*, vol.1, no.2, 2011.

Bahareh Langari received the B.S. degree in computer engineering from Islamic Azad University Tehran central branch, Tehran, Iran, in 2004 and the M.S. degree in Data Communication Systems from Brunel University, London, UK, in 2010. She is currently pursuing the Ph.D. degree in electrical engineering at Brunel University, London, UK.

Saeed Vaseghi was born in Rasht, Iran. He received the degree in electrical and electronics engineering from Newcastle University, Newcastle, U.K., and the Ph.D. degree in signal processing from Cambridge University, Cambridge, U.K.

He is a Professor of communication signal processing. He is with the Computational Intelligence and Signal Processing Research Group, University of Chemistry and Technology & Czech Technical University in Prague, Czech Republic. His research interests include speech modeling and recognition, speaker and accent morphing, and speech enhancement in noisy mobile phone environments. He has written two books: *Advanced Signal Processing and Noise Reduction* (2006) and *Multimedia Signal Processing* (2007).

Ales Prochazka received the Ph.D. degree in 1983 and has been appointed as a professor in Technical Cybernetics by the Czech Technical University in 2000. He is currently the Head of Digital Signal and Image Processing Research Group at the University of Chemistry and Technology, and the Czech Technical University in Prague. His research interests include mathematical methods of multidimensional and multichannel data analysis, segmentation, feature extraction, classification and 3D modeling with applications in biomedicine and engineering.

Babak Vaziri received the B.S. degree in computer engineering from Shahid Beheshti University, Iran, the M.S and Ph.D. degree in computer engineering from Islamic Azad University, Iran .He is currently an Assistant Professor of computer engineering at the Department of Electrical and Computer Engineering, University of Islamic Azad. Since 1998 he is a faculty member of Islamic Azad University (Central Tehran Branch). His research interests include image processing and data mining.

Farzad Tahmasebi Aria received the B.S. degree in computer engineering from Islamic Azad University Tehran Central branch, Iran, the MSc in International Marketing Management from University of East London, the MSc Business & Management from University of Bedfordshire, UK, and M.Phil. degree in computer science from Middlesex University London. He is currently pursuing the Ph.D. degree in computer science at Middlesex University London. He is a lecturer at Middlesex University London at the department of Science & Technology since 2013 and his research interests include mathematics and data analytics.